Supplementary Material (ESI) for Chemical Communications

Supporting Information

Absolute Helicity Induction in Three-Dimensional Homochiral Frameworks

Jian Zhang, and Xianhui Bu*

Department of Chemistry and Biochemistry, California State University, Long Beach, 1250 Bellflower Boulevard, Long Beach, CA 90840; E-mail: xbu@csulb.edu

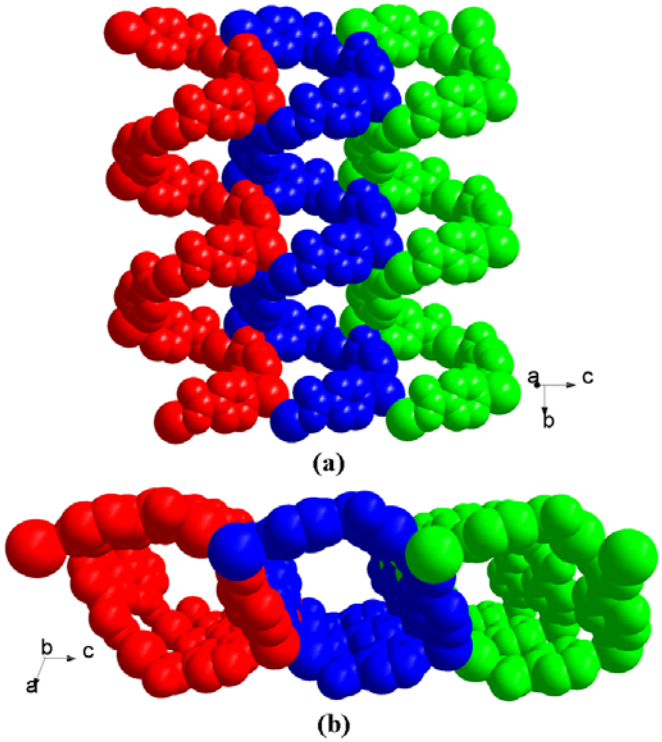

Figure S1. View of the homochiral layer based on achiral isonicotinate ligands in **1D** showing the assembly of right-handed single-stranded 2_1 helices. (a) Projected down the *a* axis. (b) Projected down the *b* axis. Adjacent helices are highlighted in red, blue and green.

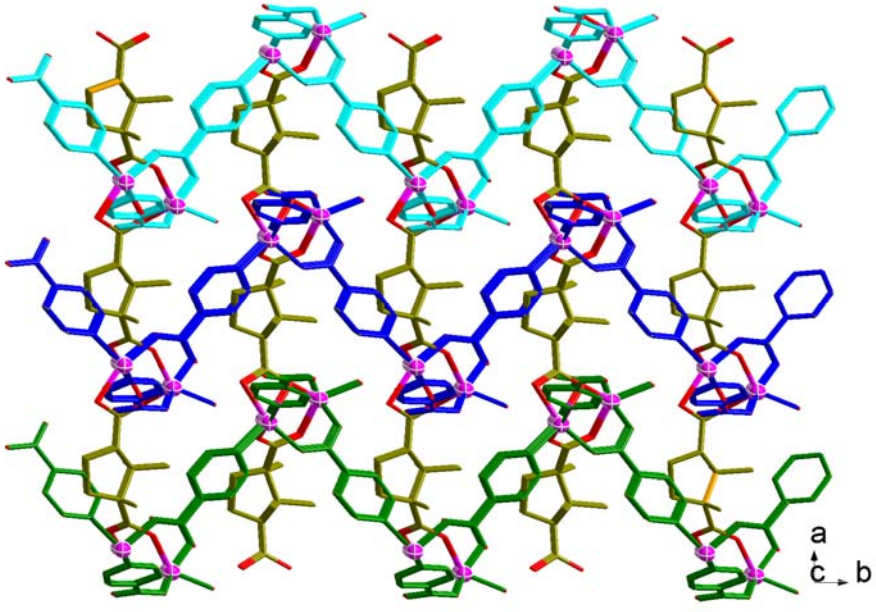

Figure S2. View of the 3D framework of **1D** along the *c* axis, showing wave-like layers (made of cobalt isonicotinate, and highlighted in cyan, blue, and dark green) joined together by D-Cam ligands along the *a* axis.

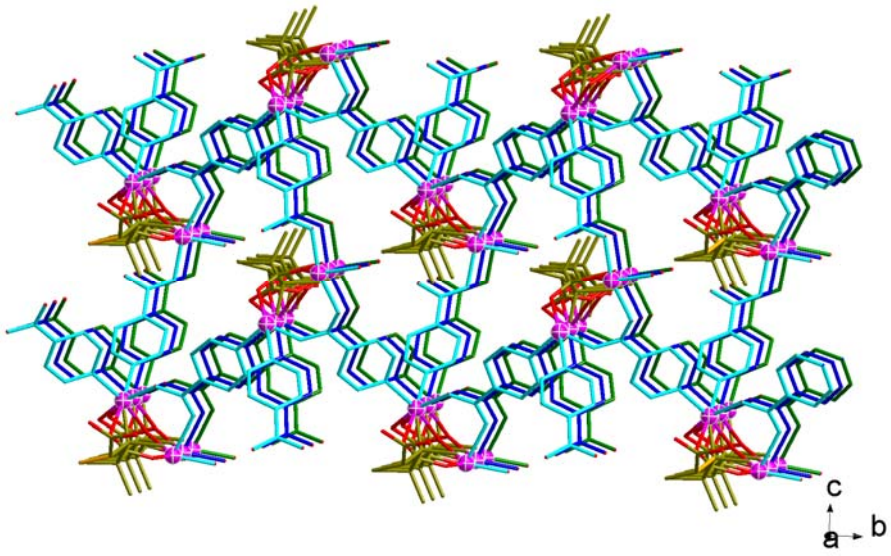

Figure S3. View of the 3D framework of **1D** along the *a* axis.

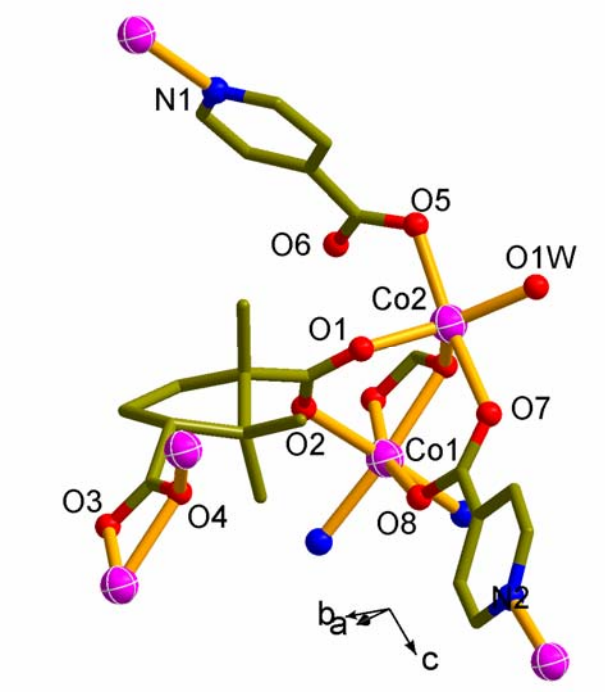

Figure S4. Crystal structure of **1L** showing the atom-labeling scheme. Hydrogen atoms were omitted for clarity.

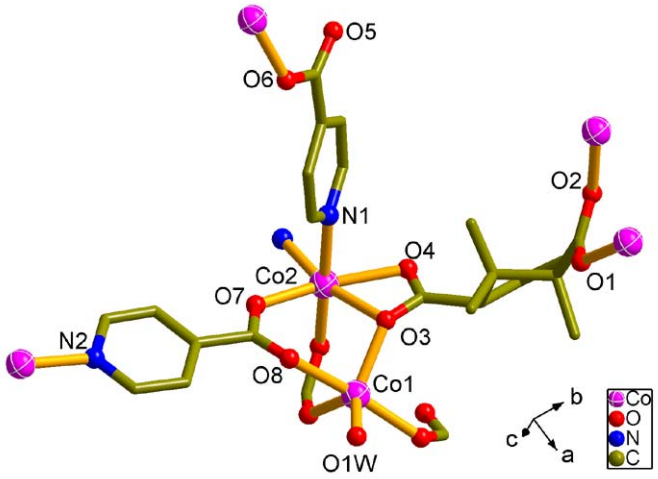

Figure S5. Crystal structure of **1R** showing the atom-labeling scheme. Hydrogen atoms were omitted for clarity.

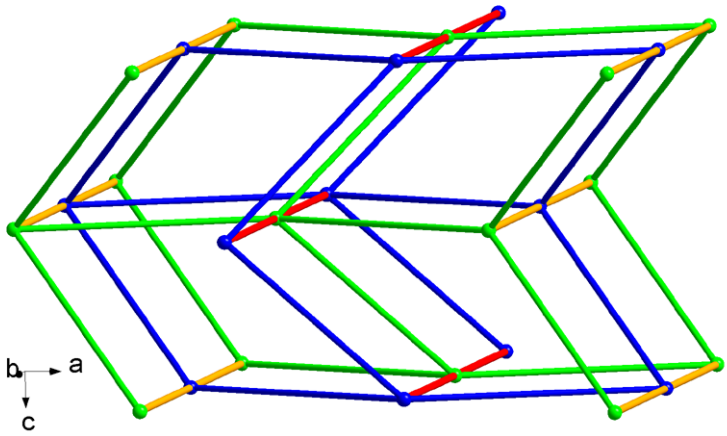

Figure S6. Topological representation of the 6-connected $4^8.6^7$ net in **1R**. Blue and green lines represent two interpenetrating diamond nets while red and orange lines represent D- and L-camphorate ligands connecting two diamond nets.

X-ray powder diffraction: X-ray powder diffraction experiments were performed on a Bruker D8 Advance X-ray powder diffractometer operating at 40kV and 40mA (CuKα radiation, λ = 1.5418Å). The data collection was carried out with a step size of 0.03 degree and counting time of 1s per step. The 2-theta angular range is from 5 to 40 degrees.

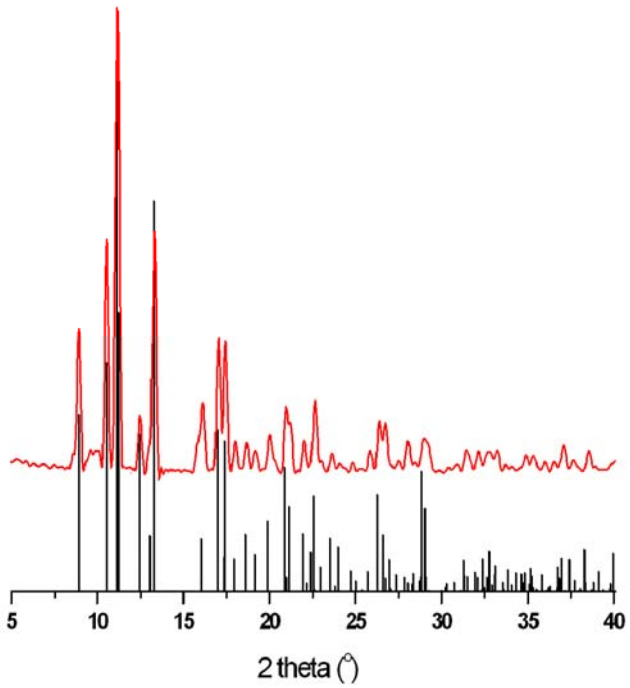

Figure S7. XPRD patterns for **1D**: (top) taken at room temperature; (bottom) calculated on the basis of the structure determined by single-crystal X-ray diffraction. The small bump at 2-theta below 10 degree suggests possible minute quantity of impurity.

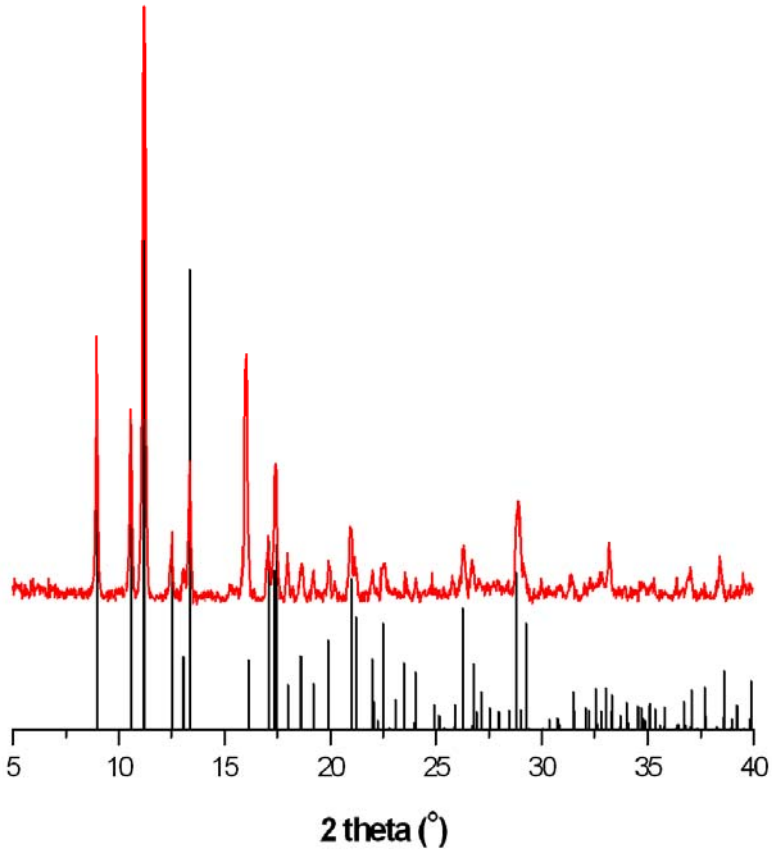

Figure S8. XPRD patterns for **1L**: (top) taken at room temperature; (bottom) calculated on the basis of the structure determined by single-crystal X-ray diffraction.

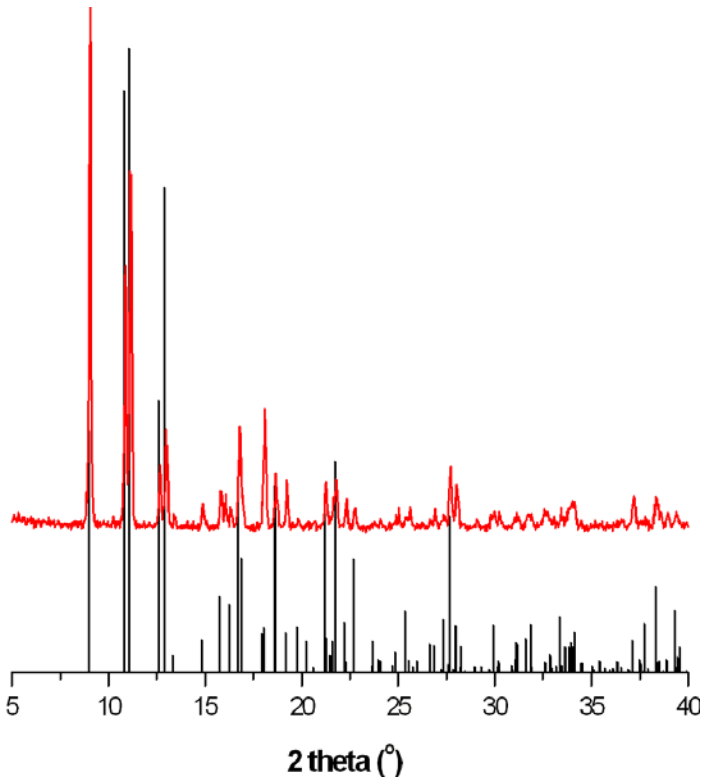

Figure S9. XPRD patterns for **1R**: (top) taken at room temperature; (bottom) calculated on the basis of the structure determined by single-crystal X-ray diffraction.

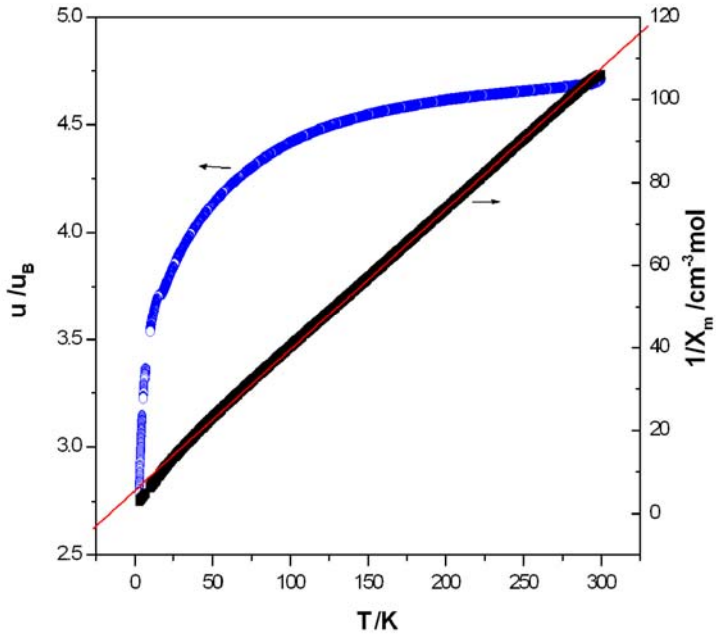

Figure S10. $1/\chi_m$ and u_{eff} vs T plot with the theoretical fit (-) for **1D**. The variable temperature magnetic susceptibility of **1D** was measured in the temperature range from 300 to 2 K, at a magnetic field strength of 5000 Oe. It can be seen that the μ_{eff} value decreases gradually upon cooling and the μ_{eff} value per metal atom at 300 K is 4.71 μ_B, which is larger than the expected spin-only value of 3.87 μ_B for a high-spin Co^{II} ion with $S = 3/2$, thus showing an unquenched orbital contribution. The magnetic data above 14 K can be fitted to the Curie–Weiss law with $C = 6.38$ cm^3 K mol^{-1} and $\theta = -16.34$ K. The C value corresponds to $g = 2.43$ with $S = 3/2$. The small negative Weiss constant suggests a weak antiferromagnetic interaction. According to the structure of **1**, the main magnetic interactions between the metal centers might happen in the dinuclear Co units, while the superexchange interactions between Co^{II} ions through the int or D-Cam bridges can be less significant owing to the length of these ligands.